Electro-optical modulators in particle detectors

T. Tsang and V. Radeka
Brookhaven National Laboratory, Upton, New York 11973

(Received 5 October 1994; accepted for publication 5 April 1995)

Results of an investigation to minimize the local electronics in particle detectors using electro-optical intensity modulators are reported. The electrical charge signals from a particle detector are first applied to a low noise electronic charge-sensitive preamplifier and the resulting signal charges are converted into optical signals using an integrated Ti:$LiNbO_3$ Mach–Zehnder interferometric optical modulator. By driving the optical modulator with a low noise diode-pumped Nd:YAG laser at a wavelength of 1.3 μm and detecting the output signals using a fast pulse shaping technique, the charge output of a particle detector can be measured at high rates with high accuracy up to 3 decades of dynamic range. The performance characteristics of such a detector signal transfer scheme, using first a single channel optical modulator and then a 16-channel integrated optical modulator array, is reported. Using the charge output from a multiwire proportional chamber, this electrical charge to optical signal transfer scheme is compared to the conventional particle detection technique. Effects of radiation dose on the optical modulator are also presented. Finally, the implication of using such an optical technique is discussed. © *1995 American Institute of Physics.*

I. INTRODUCTION

The novel concept of using optical modulators and fiber-optic cables for the readout of analog signals in high-energy particle detectors was proposed recently, and proof of principle experiments were previously done.[1–3] In this paper, we detail our analysis of a single-channel integrated electro-optical modulator and extend our application to an integrated optical modulator array for the transfer of particle detector signals. We also incorporate the recent results of direct charge transfer from a multiwire proportional chamber to a modulator and the radiation effects study of a fully packaged optical modulator. In the last section, we compare the direct signal charge transfer using such optical modulators to that of a high charge gain device, and we comment on their significance.

The signal transfer scheme using an optical device in particle detectors is an attractive alternative approach, especially in detectors having many signal channels. In the traditional signal detection scheme, charge induced on the electrodes of a particle detector is first amplified by a preamplifier, followed by a shaping amplifier, or transferred directly using electrical transmission lines to a remote location for further signal processing. Such signal transfer schemes relying on copper cables for signal transmission result in a limited bandwidth and/or cable length, and they are also vulnerable to signal cross-talk and electromagnetic interference. In systems with very many signal channels, such as detectors for large hadron colliders, identifying the signal information at the trigger level with a high degree of parallelism in signal transfer and processing, the readout electronics using the traditional technique becomes rather complex and is almost a formidable task. The electro-optical concept utilizes a system of Mach–Zehnder optical intensity modulators, fabricated on a single substrate, and powered by a 1.3 μm cw laser source. In one scheme, signal charge from a detector may be applied directly to the electrodes of the modulator. Alternatively, charge is fed first to a preamplifier and the output signals are then applied to the electrodes of an optical modulator. Laser light is brought in from a remote source on a single-mode polarization preserving fiber, and the optical output signals are carried on ribbon single-mode fibers. This approach may dramatically reduce the mass–volume in detectors with many signal channels by eliminating copper cables, increase the signal bandwidth, improve the noise immunity, and provide a high radiation resistance. Furthermore, the capability of operating the optical modulators in a cryogenic detector such as a liquid ionization calorimeter also simplifies the cold feedthroughs and lowers the heat loss due to copper cables. Optical modulators are passive devices that do not generate heat. However, there is some amount of optical power loss into the substrate due to branching loss and coupling loss. Yet the heat dissipation of the modulators is still less than that of the conventional electronic devices. The capability of summing all detector signals optically rather than electronically to deduce the total energy collected by a detector prior to any electronic signal processing may also be attractive in some applications.

II. CHARACTERIZATION OF THE OPTICAL MODULATOR SYSTEM

A. Optical modulator

1. Single-channel optical modulator

The optical modulator is fabricated on a single crystal of $LiNbO_3$, with titanium in-diffused waveguide structures integrated in a Mach–Zehnder configuration. The principle of operation is based on the linear electro-optic effect or the Pockels effect: a change of optical birefringence (refractive index) in the waveguide due to application of an electric field. Several commercially available titanium in-diffused optical modulators have been used, all performing well at room temperature. In this particular work, annealed-proton-exchange x-cut y-propagating Ti:$LiNbO_3$ optical modulators were employed. Fabrication details of such annealed-proton-exchange devices can be found in several references.[4] A

 0034-6748/95/66(7)/3844/11/$6.00

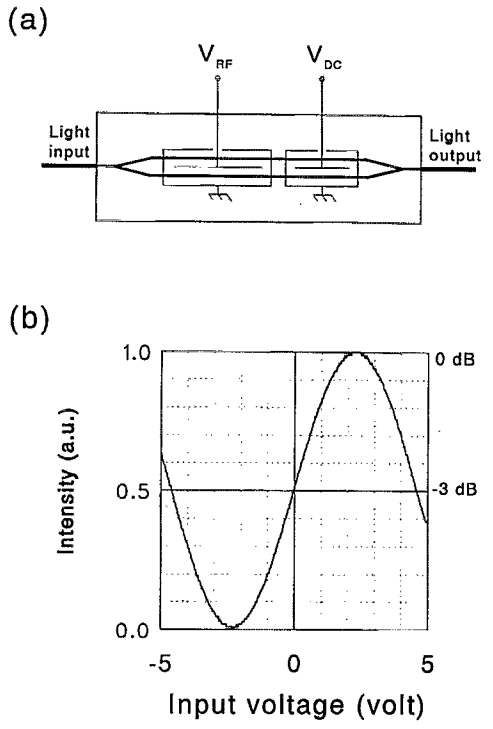

FIG. 1. (a) The schematic of a Mach–Zehnder optical modulator with separate electrode for bias control. (b) The transfer characteristic of the optical modulator—the interferometric fringes as a function of the applied voltage.

schematic of this type of intensity modulator is shown in Fig. 1(a). A polarized light beam traveling in a single transverse-mode optical waveguide is split by refraction into two beams, carried a suitable distance, and then recombined, giving rise to interference. The interference is constructive when the two beams are in phase, and the full power exits to the output waveguide. If the optical lengths of the two arms differ by half of a wavelength (optical phase of π), the interference is destructive, and the optical power is lost by radiation into the substrate. A recent advance in the design of modulators has been to terminate the exit end of the Y junction by a 3 dB coupler, thus producing two complementary optical outputs with no power loss, hence no thermal loading to the substrate which would significantly relax the thermal budget in a particle detector. A push–pull-type rf-signal electrode and a dc-bias electrode are separately defined on the waveguide structure. The modulator is pigtailed with a single-mode polarization maintaining fiber at the input end and a standard single-mode fiber at the output end. Both fiber ends are terminated with ST (AT&T registered trademark) fiber connectors. A change of the refractive index of the waveguide resulting from the application of an electrical signal to the electrode causes an optical phase shift, hence intensity changes in the output of the interferometer. Figure 1(b) shows a portion of transfer characteristics of the modulator. The optical output power of the modulator is a well defined function of the half-wave voltage V_π; in our present definition of parameters, it is given by

$$\frac{\text{power out}}{\text{power in}}=\frac{1}{2}\left[1+\sin\left(\frac{V}{V_\pi}\right)\right]\simeq\frac{1}{2}\left[1+\frac{V}{V_\pi}\right], \tag{1}$$

where V is the modulation voltage and the approximation is valid for $V\ll V_\pi$. At the operating point of zero voltage bias, the output intensity is at -3 dB. The single-channel modulator has an extinction ratio in excess of 23 dB, an insertion loss of 7 dB including coupling loss, and a 3 GHz electrical bandwidth. V_π is 4.5 V and the electrode capacitance C_A is 14 pF over a length of 10 mm. Therefore the resulting switching charge $Q_\pi=C_AV_\pi$ is 63 pC, and is independent of the electrode length l because $V_\pi\propto l$ and $C_A\propto 1/l$. It is important to note that modulators with smaller V_π and lower input capacitance will improve the sensitivity of charge measurements. Also, placing the modulator close to the electrode of the particle detector is essential in order to reduce the overall capacitance, when coupling directly to the detector without using a preamplifier.

The dynamic range of the optical modulator will be determined by the requirement on linearity, while the nonlinearity of the modulator operating in the quasilinear regime can be determined explicitly from its response function. For a 1% maximum deviation from a tangent through the -3 dB point, the maximum signal $V_{\max}\approx 0.25V_\pi/\pi$, or 360 mV in the present case, and the corresponding maximum signal charge $Q_{\max}$ is 5 pC. If the system noise reaches quantum limit and is dominated by the photon statistics as discussed in the next section, the dynamic range with respect to the photon noise is given by[1]

$$\frac{V_{\max}}{\sigma_{\rm rms}(V)}=\frac{Q_{\max}}{\sigma_{\rm rms}(Q)}=0.25\,\frac{Q_\pi}{\pi}\,\frac{1}{\sqrt{n_0a_Ft_m}}. \tag{2}$$

Here $\sigma_{\rm rms}(V)$ and $\sigma_{\rm rms}(Q)$ are the rms noise voltage and the equivalent noise charge, respectively, n_0 the received photoelectron rate at the photodetector, t_m the integration time of the shaping amplifier (40 ns), and a_F a filter parameter, equal to 1.55 with the present bipolar shaping amplifier configuration. Many active[5] and passive[6] linearization schemes have been adopted to further enhance the linearity of the modulator response, in particular, for cable television application where higher-order distortion is limited to -80 dB. The dynamic range and the integral linearity of the optical modulator are shown in Figs. 2(a) and 2(b), respectively, where an ac electrical signal is applied at the -3 dB point to the electrode of the modulator and the modulated output optical signal is recorded and normalized. The deviation from the 1% integral linearity on the transfer characteristic of the optical modulator is indeed observed at the input signal level of $\sim$300 mV with a dynamic range exceeding 10^3. Although the nonlinear response of the optical modulator is well defined and very large signals could conceivably be analyzed with even higher dynamic range by observing the output signals over multiple fringes, this technique would complicate the detection electronics.

The short-term and long-term thermal stability of the titanium in-diffused modulators has been actively pursued in recent years[7–10] while proton-exchange devices[4] are currently being examined.[11] Because the pyroelectric coefficient is about an order of magnitude smaller in the x-cut than in the z-cut devices,[12] the dc drift phenomena in the x-cut Ti:$LiNbO_3$ are less pronounced and good short-term stability

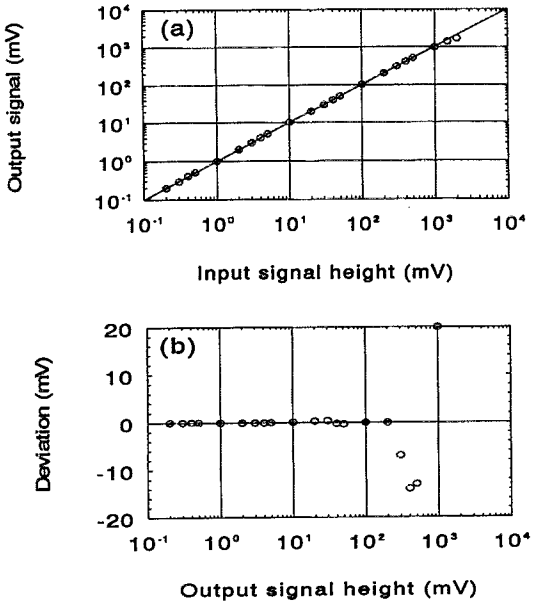

FIG. 2. (a) The dynamic range and (b) the integral linearity of a single-channel optical modulator.

can be achieved. In the present experiment, the device is operated at room temperature at the -3 dB point with a constant dc bias but without active dc-bias control stabilization. The short-term thermal stability (few hours) of the proton-exchange optical modulator is found to be $\pm 0.01\ \pi$ phase drift which is relatively small; therefore the experiment is conducted without any active stabilization.

2. Optical modulator array

Many electronic signal channels are generally presented in a particle detector. In order to examine the possibility of using an optical technique for transfer of signals from detectors with many readout channels, we have extended our studies to arrays of integrated optical modulators.

Sixteen optical modulators are fabricated on a single substrate and fully packaged by AT&T. The modulators are defined on a z-cut single crystal of $LiNbO_3$ substrate, with titanium in-diffused single-mode waveguide structures integrated in a Mach–Zehnder configuration. Input optical power is distributed by a binary waveguide tree on the substrate from a single waveguide to the 16 modulator channels. The details of the optical power fan-out are shown in Fig. 3. Electrodes are defined on the arms of each modulator with a square shaped gold pad for wire bondings. The modulator arrays are pigtailed with single-mode polarization preserving fiber at the input end and single-mode ribbon fiber at the output end; all fiber ends are terminated with ST fiber-optic connectors. All channels have a half-wave voltage of 5.4 ± 0.05 V, which it is slightly larger than the V_π of the previously described single-channel modulator. The waveguide branching angle is carefully designed to minimize the insertion loss, Considering a 12 dB (4×3 dB) branching loss per channel, 0.2 dB loss per splitting, 6 dB propagating loss per channel over a length of 7 cm, and 0.5 dB loss per optical coupling, adding to a total of 20 dB insertion loss per modulator channel. Figure 4 shows a measured insertion loss of 22.5 ± 0.4 dB across all modulator channels except channel 1, which has a defect (a small chipping) on the substrate near the exit end of channel 1. Other modulator arrays later tested have insertion losses varied from 21 to 22.5 dB which are in reasonable agreement with prediction. The extinction ratio reached 21.5 ± 2.5 dB (see Fig. 4), indicating that the polarization axis of the PM fiber is well matched to the input waveguide. The electrical cross-talk, measured at 10 kHz on

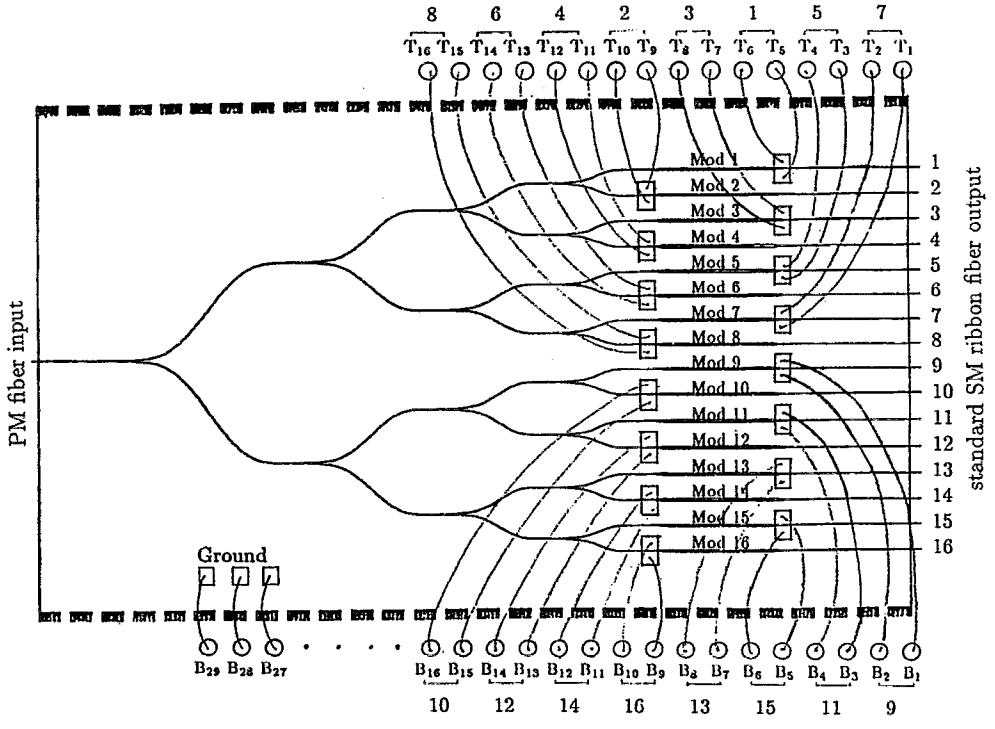

FIG. 3. Details of the optical power splitting on the optical modulator array. The y axis is magnified 10× to that of the x axis.

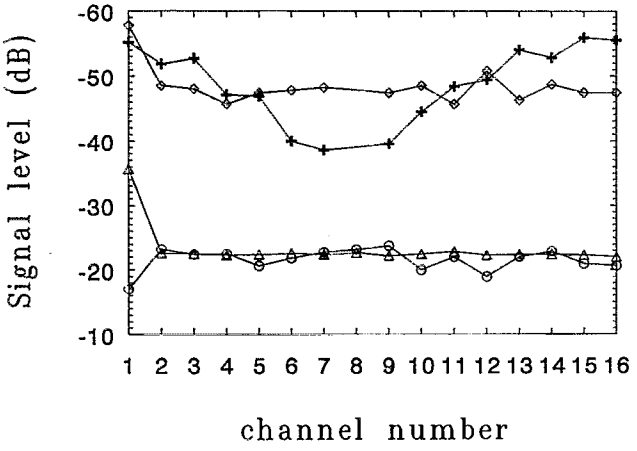

FIG. 4. The insertion loss (△), extinction ratio (○), cross-talk (+), and reverse optical isolation (◇) of a 16-channel optical modulator array.

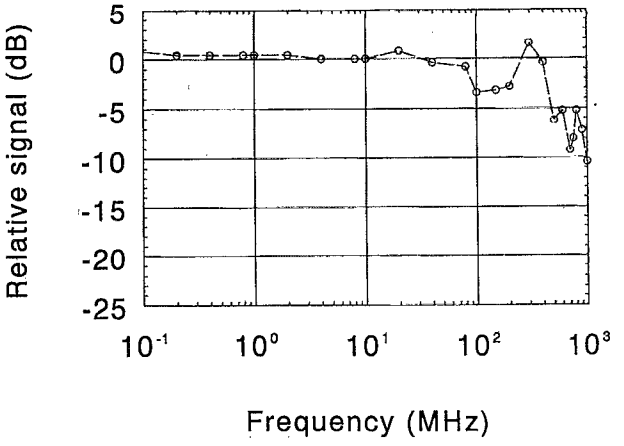

FIG. 5. The frequency response of a 16-channel optical modulator array.

the next-to-nearest-neighbor channel electrode, is below −40 dB and decreases to −55 dB at the furthermost neighbor channels; see Fig. 4. Since the electrical cross-talk transferred directly and linearly to the optical response, the optical cross-talk would resemble that of the electrical and was confirmed by measuring the optical output at the next-to-nearest channel. There is a possibility of interference by the next-to-nearest-neighbor channel through optical coupling at the optical splitter or by acoustic means. Such optical isolation was measured by coupling a modulated laser beam at the fiber exit end of modulator channel 8 (reversing the coupling direction) while detecting the optical signal received on all other channels using a lock-in amplifier, and the results are shown in Fig. 4. If reverse optical coupling through the splitter is dominant, one would anticipate a significant drop in optical power with increasing number of splittings. However, a flat >45 dB isolation across all channels was observed, indicating that the measured optical signal may originate from an acoustic rather than an optical source. Since the propagation loss of acoustic phonons is merely a couple of decibels per centimeter and the entire transverse length of the modulator channel is only 4 mm, acoustic phonons are conceivably capable of coherent coupling to all other modulator channels without much loss in amplitude. The frequency response of the modulator array has a −3 dB cutoff at ~100 MHz (see Fig. 5) and it is mostly limited by the lumped electrodes and the long gold wire bondings (also see Fig. 3). Because the signal passband of the photodetector–receiver is centered at a few megahertz where the frequency response of the modulator is flat, the present modulator array is adequate for signal transfer.

There have been concerns about the optical power handling capability of the integrated optical modulator arrays. High optical power up to 400 mW has been tested only on single waveguides. Because some optical power loss is anticipated in the modulator, more than 400 mW of optical power may be required to drive the 16-channel modulator array to yield a photocurrent of 1 mA per modulator channel for electronic signal transfer. Furthermore, good optical finish at the input end of the waveguide is essential to ensure a high optical damage threshold. High quality of the waveguides with minimum defects will lower the possibility of optical ionization at high optical power levels. Figure 6 shows the optical power handling capability of two 16-channel optical modulator arrays. A high power fiber-coupled diode-pumped Nd:YAG laser (Adlas model DYP-423-FP), which has a maximum optical power output of 850 mW at the wavelength of 1.3 μm, was employed. Greater than 500 mW of optical power is coupled to one of the modulator arrays, resulting in >4 mW power output per modulator channel available for signal transfer, and provides a factor-of-2 safety margin in optical power for maintaining the 1 mA photocurrent per signal channel standard. Using the full optical power output of this high power laser, four optical modulator arrays with outputs of 1 mA photocurrent per channel, that is, a total of 64 signal channels, can be driven simultaneously using a single photon source.

B. Laser sources

For experiments performed on a single-channel optical modulator, a low power diode-pumped cw Nd:YAG laser was used. The laser is linearly polarized with 30 mW power output at the fiber end. A −30 dB Faraday isolator is built

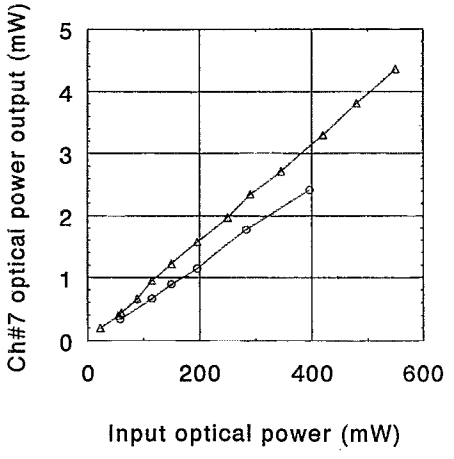

FIG. 6. The optical power handling capability of two 16-channel optical modulator arrays.

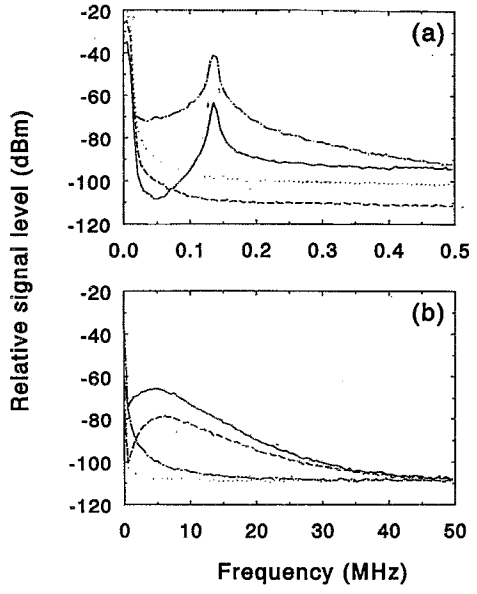

FIG. 7. Noise spectrum of the photodetector–receiver with and without the application of a 1 mA photocurrent. (a) Frequencies span from dc to 0.5 MHz and (b) from dc to 50 MHz. The lines are depicted as: (···) noise floor of the preamplifier, (---) noise floor of the preamplifier and the shaping amplifier, (-·-) noise spectrum of 1 mA photocurrent amplified by the preamplifier, (—) noise spectrum of 1 mA photocurrent amplified by the preamplifier followed by the shaping amplifier.

into the laser and the output end is pigtailed to a 50 m long uncoated polarization maintaining fiber terminated with ST connectors. Less than −158 dB/Hz of relative intensity noise (RIN) is measured at frequencies above 1 MHz. However, the laser is not equipped with feedback electronics for suppressing the intensity noise caused by the relaxation oscillations of the Nd:YAG crystal, which is centered at 140 kHz and with excess noise extending close to the megahertz region; see Fig. 7(a). The RIN level of this relaxation oscillation at the frequency of 140 kHz is less than −100 dB/Hz. This excess laser noise can be suppressed with an appropriate feedback stabilization, but it was not used here. Instead, by using a 40 ns peaking time bipolar pulse shaping technique, the relaxation oscillations are filtered out without substantially affecting the signal pulse received by the photodetector–receiver. We noted that the drive laser of the 16-channel modulator array, a 850 mW power output diode-pumped laser, emits a similar noise spectrum but with some small level of excess noise spiking at various frequencies below 1 MHz and is attributed to the noise of the power supply. We comment further on the laser sources and the excess noise suppression below.

Although the diode-pumped Nd:YAG laser system is known to be an ideal low noise photon source for many applications, its intense intrinsic relaxation oscillation at ~140 kHz presents some problems to single event detection, such as particle detection. Many feedback approaches have been employed to reduce this noise propagating to the photodetector–receivers by stabilizing the photon source or by inserting appropriate electronic bandpass filters at the postamplifier stage. Our selection of using a low noise bipolar shaping amplifier at the receiving end with a peaking time of 40 ns has effectively filtered out the low-frequency components with minimum effect on the signal output. A qualitative analysis of the photon noise using a photodetector–receiver and a rf spectrum analyzer is first given here. Spectrum analysis of this photodetector–receiver with and without the application of a 1 mA photocurrent is illustrated in Fig. 7(a) and 7(b), with rf frequencies from dc to 0.5 MHz and from dc to 50 MHz, respectively. In all of these measurements a Tektronics 2797 spectrum analyzer is used; the measurement bandwidth is set at 10 kHz. The relaxation oscillation of the Nd:YAG is clearly seen at 140 kHz with a relative power level of −41 dBm measured at the output of the preamplifier (dotted–dashed lines) and −63 dBm at the output of the shaping amplifier (solid lines). A reduction of 22 dBm is obtained after being filtered by the shaping amplifier. The signal bandwidth of the photodetector–receiver, which includes the photodiode, preamplifier, and the shaping amplifier, is centered around 5 MHz [dashed line of Fig. 7(b)] and is very much isolated from the broad 140 kHz relaxation oscillation. Therefore single event detection approaching shot-noise-limited noise level may be achieved. The frequency spectrum of the noise of a 1 mA photocurrent is clearly observed at the output of the photodetector–receiver, that is, at the output of the shaping amplifier, solid line of Fig. 7(b). Although the RIN presented in the laser source is low, <90 dB/Hz, it constantly modulates the signal in a random manner giving rise to a *modulating noise*. We will discuss this further in the next section.

C. Photodetector–receivers

A quantitative analysis of the noise of the photodetector–receiver is given in this section. The modulator system noise imposes a lower limit on the charge-sensitivity measurements. Indeed, the system noise is dominated by the photon statistics and the excess photon noise in the present experiment; the low noise of the photodetector–receiver contributes only a small amount to the equivalent noise charge. Consider the experimental setup shown in Fig. 1(a), but with the rf port of the optical modulator grounded and a dc-bias voltage set to the operating point. The photodetector–receiver noise and the laser noise can be determined within the signal bandwidth of the photodetector–receiver, which is the only frequency band of interest [see Fig. 7(b)] in this part of the experiment. A calibrated charge is injected into the preamplifier; the output pulse height from the shaping amplifier and the corresponding rms noise voltage are recorded. The rms noise voltage is then measured after switching on a known amount of photocurrent. The heavy solid line of Fig. 8(a) shows a calibrated signal pulse height of 26.6 mV when a step voltage of 10 mV is applied to a 3 pF capacitor, that is, a 30 fC charge injection, at the input of the preamplifier. By displaying an envelope of 256 signal traces, an rms noise voltage of 0.91 mV is measured at the base line of the signal trace. This noise voltage corresponds to an equivalent noise charge of 1.03 fC or 6.4×10^3 rms electrons. The noise charge includes the photodiode noise (dark current of 2 nA) and the preamplifier and the shaping amplifier noise. A numerical value of the charge collection time $a_F t_m$ (shot-noise integral) of the photodetector–

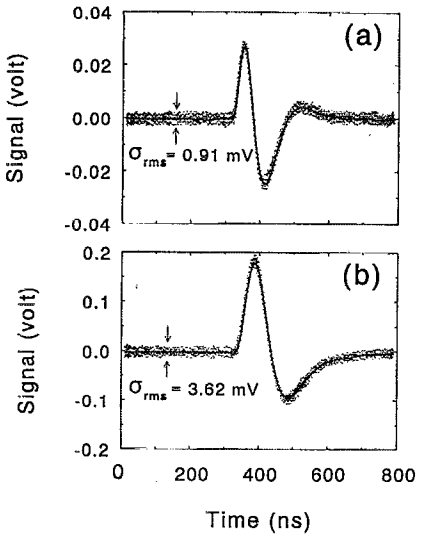

FIG. 8. (a) The calibrated signal pulse from the photodetector–receiver with the application of a 10 mV step voltage to a 3 pF capacitor at the input of the preamplifier—corresponds to 30 fC charge injection. (b) The signal pulse received by the photodetector–receiver when a 10 mV step voltage is applied to the rf electrode of the optical modulator. The dark solid lines are the average of the 256 signal traces displayed. Notice that the y-axis scales are not the same in both figures.

receiver is computed using this calibrated wave form. An equivalent shot-noise integral of 62 ns is obtained by performing the integration $a_F t_m = [\int |f(t)|^2\, dt]/N^2$, where $f(t)$ is the wave-form function and N is the measured peak height.[13] When 1 mA of photocurrent is received by the photodetector–receiver at the integration time of 62 ns, the number of photoelectrons received is 3.875×10^8. Therefore the theoretical shot-noise-limited photoelectrons yields $\sigma_{\rm rms}^{\rm theory}(Q)=19.6\times10^3$ rms electrons. The number of photoelectrons produced at the receiver during the measurement time t_m by a step in the modulator input voltage is

$$t_m \Delta n = \pi \frac{\Delta V_{\rm in}}{V_\pi} t_m n_0, \tag{3}$$

where Δn is the change in photoelectron rate caused by an applied voltage of $\Delta V_{\rm in}$. We obtain the equivalent input noise voltage from Eqs. (1) and (2) by substituting $t_m \Delta n = \sigma(n) = \sqrt{a_F n_0 t_m}$ and $\sigma_{\rm in}(V) = \Delta V_{\rm in}$:

$$\sigma_{\rm in}(V) = \frac{V_\pi}{\pi} \sqrt{\frac{a_F}{n_0 t_m}}. \tag{4}$$

Experimentally, the photon noise of a 1 mA photocurrent propagating through the photodetector–receiver is observed. Figure 8(b) shows an envelope of 256 signal traces of the shaping amplifier output when a 10 mV step voltage is applied to the optical modulator. If one estimates the excess noise from the base line of the signal, an excess rms noise voltage of 3.62 mV is measured. This noise voltage corresponds to an equivalent noise charge of 4.09 fC or 25.6×10^3 rms electrons. Therefore a measured photon noise charge $\sigma_{\rm rms}^{\rm exp}(Q)$ of 24.8×10^3 rms electrons is obtained [$\sigma_{\rm rms}^{\rm exp}(V) = \sqrt{3.62^2-0.91^2}$ mV], which is 1 dB above the theoretical shot-noise limit. This 1 dB excess photon noise includes the contribution of the thermal noise of the optical modulator and the intensity noise caused by the residual relaxation oscillation of the laser. The dielectric noise[13] of the optical modulator is given by $\sqrt{2.4kTDC_A}$, where D is the dielectric loss factor, k the Boltzmann constant, and T the temperature, and is less than 500 rms electrons. It seems that the shaping amplifier has filtered out a significant portion of the relaxation oscillation frequency of the laser and approaches the theoretical shot-noise-limited detection sensitivity. However, shaping amplifiers with longer shaping time constants, which in principle would have better noise reduction, do not filter out this strong relaxation oscillation effectively.

Excess noise estimated from the base line of a signal pulse is generally acceptable in conventional detector signal processing; however, in this particular experiment the approach is not strictly correct in determining the excess photon noise presented in the signals. Because the increase in magnitude of a signal pulse is a consequence of increasing photon detection, there is an increase in excess photon noise other than the noise of a 1 mA photocurrent that is inherently associated in all signal pulses. At the largest voltage pulse of 360 mV applied to the optical modulator operating at the −3 dB point with 1 mA of photocurrent received at the photodetector–receiver, a peak photocurrent of 1.25 mA is actually contained at the signal pulse. That is, approximately 0.5 dB more photon statistics is measured at the signal peak as compared to its base line. Therefore slightly higher photon statistics and inevitably more excess photon noise as well is anticipated at the peak of the larger signal pulses than smaller pulses. In addition to the noise due to photon statistics, the RIN of the laser also cause some *modulation noise*. Such modulation noise has progressively larger effects on larger signal pulses. To examine this phenomenon the modulated signal pulses are measured at various output levels. The values of the rms noise are calculated from the base lines and the distributions of the pulse height are recorded. Figure 9(a)–9(c) is the modulated signal pulses and Fig. 9(d)–9(f) is the calibration pulses at the equivalent output signal level of each corresponding signal pulse. The insets are the corresponding pulse-height distributions recorded on a conventional pulse-height analyzer after stretching the electronic signal pulses from ~50 ns to a few microseconds in duration. The excess photon noise can be calculated after the electronic noise of the photodetector–receiver is fully taken into account by spectrum deconvolution, that is, deconvoluting the pulse-height spectra of each signal in the insets of Fig. 9(a)–9(c) with respect to their corresponding response spectra (calibration spectra) in the insets of Fig. 9(d)–9(f) and note that FWHM$=2.35\sigma_{\rm rms}$. Agreement with the photon statistics to within 1 dB is observed at output signals <200 mV level. Larger disagreement to 2.5 dB above the photon statistics is found at the highest 2 V output signal level. Considering 1 dB due to the actual photon noise, the 1.5 dB excess noise measured at the highest peak of the signal pulses is attributed to the 140 kHz modulation noise of the laser source.

The dynamic range calculated from Eq. (1) gives a theoretical value of 1580 at the receiving photocurrent of 1 mA. However, a measured value of ~550 is obtained and is lim-

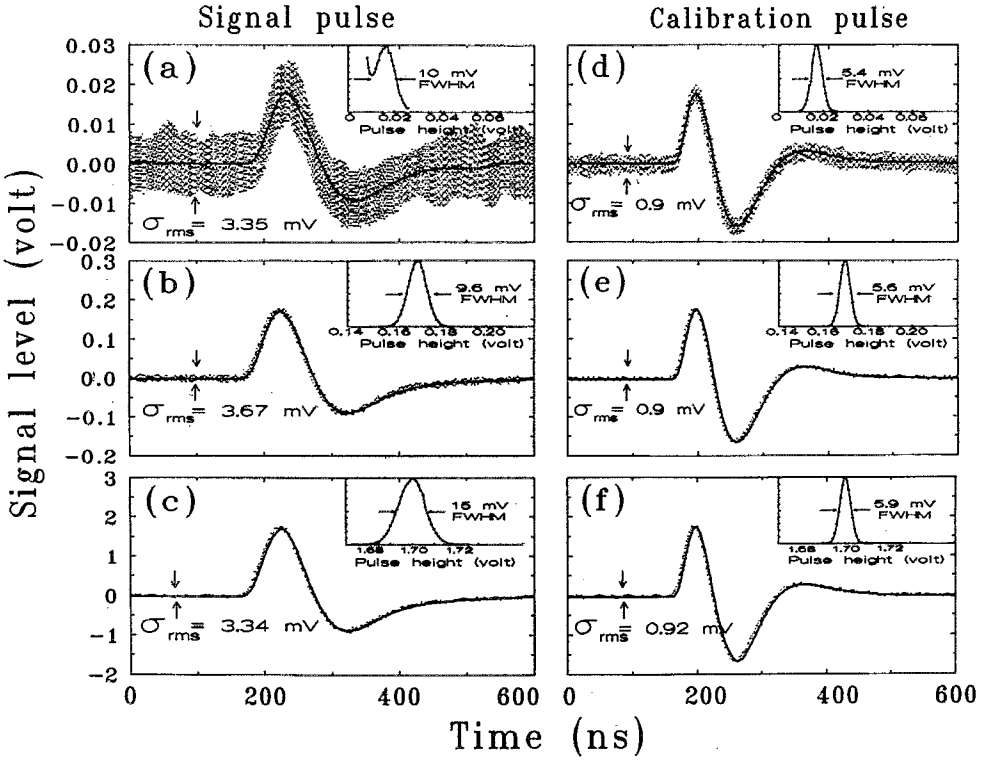

FIG. 9. (a)–(c) The modulated output signal pulses at various voltages applied to the optical modulator; (d)–(f) the calibration pulses, response of the photodetector–receiver, at the equivalent output voltage level of each corresponding signal pulse. The insets are the corresponding pulse-height distributions, and the values of the rms noise calculated from the base lines of each signal pulse are also shown.

ited only by the maximum voltage swing (high gain) of the present shaping amplifier (up to 2 V output with a measured σ_{rms} of 3.6 mV), but not by the onset of the 1% nonlinearity of the optical modulator, Fig. 10(a). The integral linearity of the present optical modulator system, which includes the optical modulator and the photodetector–receiver, approaches 1% and is shown in Fig. 10(b). We should note that the dynamic range of the optical modulator and the signal-to-noise ratio increase as the square root of the injected optical power, which could be increased somewhat. For practical and economical reasons, we have limited the optical power to ~1 mW per modulator channel with a resulting dynamic range of 10^3.

III. CHARGE MEASUREMENTS

In this study, the charge signal from a detector electrode (anode) of a multiwire proportional chamber (MWPC) is measured in three different schemes: (a) a preamplifier followed by a shaping amplifier—the conventional approach; (b) a preamplifier followed by the optical modulator; (c) detector electrode connected directly to the optical modulator. In (b) and (c) the optical signal is then detected by a photodiode followed by a preamplifier and a shaping amplifier. The detection schemes labeled (a)–(c) are noted in the subsequent figures. The experimental arrangement comprises a multiwire proportional chamber (BNL), a commercial diode-pumped Nd:YAG laser at the wavelength of 1320 nm (Amoco), a Mach–Zehnder interferometric modulator (United Technologies Photonics), a low noise fast InGaAs

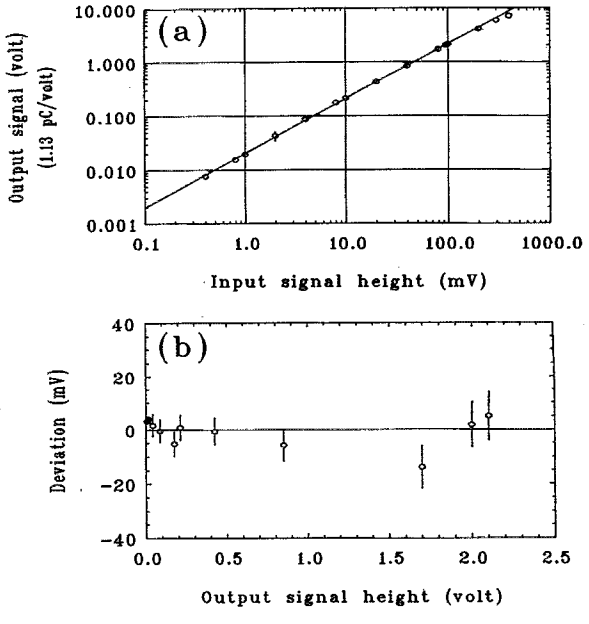

FIG. 10. (a) The dynamic range and (b) the integral linearity of the optical modulator system, which includes the optical modulator and the photodetector–receiver. 1 V of output signal corresponds to 1.13 pC of signal charge. The onset of the nonlinearity above the 2 V level signal output is mostly limited by the photodetector–receiver but not the optical modulator.

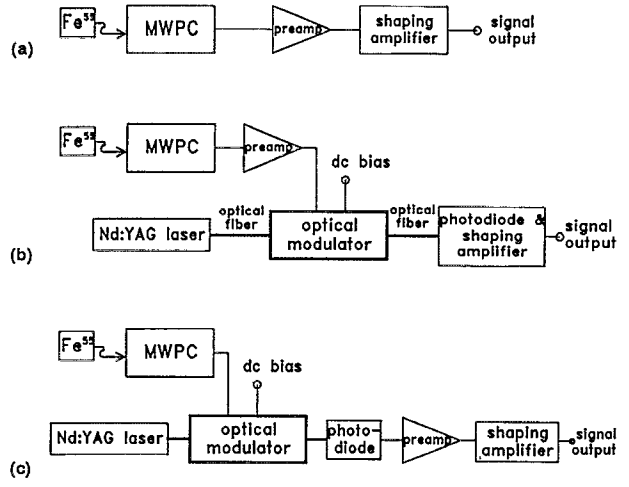

FIG. 11. Schematics of the charge measurements from a detector element of a multiwire proportional chamber, (a) a conventional approach, (b) to a preamplifier and to the optical modulator, and (c) directly to the electrode of the optical modulator. The preamplifier in (a) and (b) is BNL IO-535; a modified BNL IO-354 preamplifier is used in (c) for handling higher signal currents. The bipolar shaping amplifier is BNL IO-636 with 40 ns peaking time.

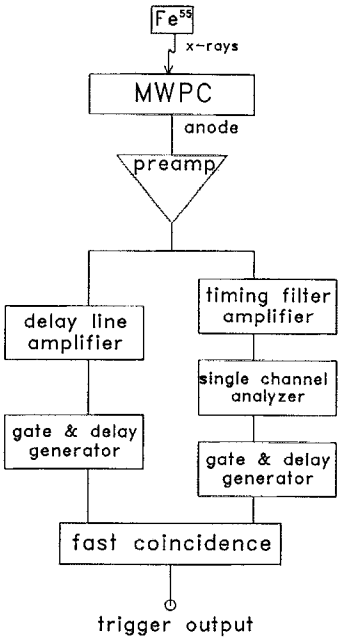

FIG. 12. The schematic of the jitter-free trigger signal.

photodiode (Hamamatsu), a low noise charge-sensitive preamplifier (BNL-535), and a bipolar shaping amplifier with 40 ns peaking time (BNL-636). Figure 11 gives the block diagram of the experimental setups.

The laser output fiber end is connected to the Mach–Zehnder modulator and the output end of the modulator is connected to a photodetector–receiver. A dc bias is applied to the modulator at the dc-bias port to shift the operating point to the -3 dB operating point (quadrature point). The laser intensity is adjusted at the quadrature point to give a photocurrent of 1 mA on the receiving photodiode. To induce the ionization, a Fe^{55} radiation source is placed in front of the window of the MWPC filled with an argon gas mixture. During the decay of Fe^{55}, x rays with energy primarily at 5.9 keV are produced and then sensed by the chamber (together with a cosmic ray background). The ionization of the argon liberates electrons and positive ions; they are collected by the anode and the cathode electrodes, respectively. Since the induced charge is generally small, low noise preamplifiers are usually required as the front end electronics. Referring to the arrangement of Fig. 11(a), a preamplifier is used to convert the anode charges to a signal voltage, and the resulting signal is used to generate a jitter-free trigger source using a fast coincidence counting technique as shown in Fig. 12. The cathode charges are fed to a separate preamplifier followed by a bipolar fast shaping amplifier, to reduce the duration of the signal pulse and to limit the detection bandwidth for noise reduction. A 10 fC test charge is then injected to the preamplifier to calibrate the output signal, shown by the dashed line of Fig. 13(a). By varying the anode voltage, the amount of charge produced in the MWPC can be controlled and the resulting signals are recorded; the solid line of Fig. 13(a) indicates a 7 fC charge output. In this manner, a charge calibration is generated and plotted in Fig. 14. It is then used as a reference chart for the subsequent experiments.

In the next arrangement shown in Fig. 11(b), a known amount of charge from the MWPC is fed to a preamplifier and then to the rf port of the optical modulator. We should note that apart from an increase of 3 dB in signal level, equal performance is found when the modulator is tested with or without 50 Ω termination on the signal electrode (that is,

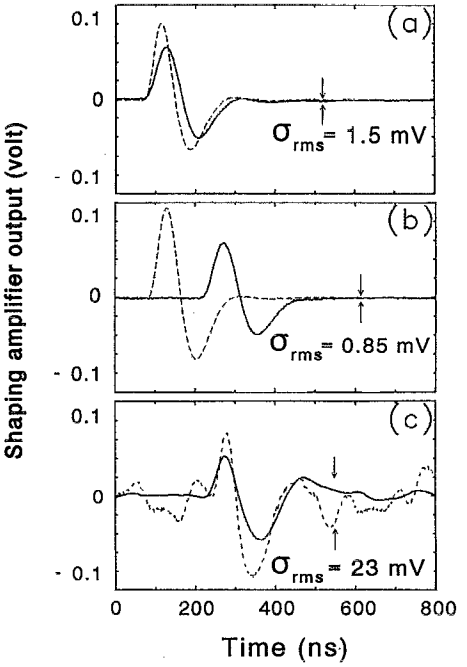

FIG. 13. The signal pulses (a)–(c) of the photodetector–receiver using the three charge measurement schemes shown in Fig. 4(a)–4(c), respectively. In (b) and (c) dashed lines are the calibrated signal pulses and the solid lines are the received signal pulses—single trace with no signal averaging. The dotted line in (c) is a typical single signal pulse and the solid line is the average of 64 signal output traces. The rms noise voltages depicted in each figure are measured using the built-in extended features of the digital oscilloscope but at a higher vertical gain.

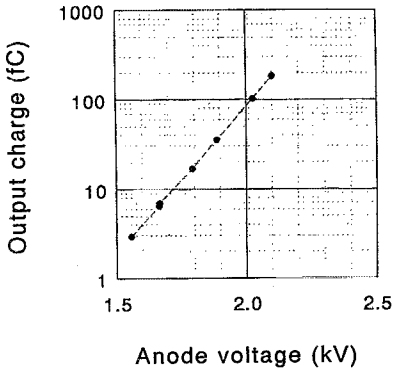

FIG. 14. The charge calibration of the MWPC obtained by varying the anode voltages.

signal applied either to the rf port or to the dc port). The modulated optical signal is received by a photodiode and the photocurrent is then fed to a receiver preamplifier followed by a fast shaping amplifier. The solid line in Fig. 13(b) shows the received signal pulse, and the dashed line shows a calibrated pulse when 100 fC charge is applied to the test port of the preamplifier. The amplitude of the output signal pulse is recorded at different anode voltages—various charge injections to the preamplifier. Using the calibration chart shown in Fig. 14, the results are plotted in Fig. 15. In this figure, the data sets depicted in (a) and (b) illustrate the linearity of the photodetector–receiver. Over 2 1/2 decades of dynamic range are measured and are limited only by the maximum voltage swing (i.e., gain) of the shaping amplifier and the available output charges in the MWPC. The noise detection level is shown by the $2\sigma_{\text{rms}}$, which is the lowest data point shown in each data set. Notice that by using identical electronics the efficiency of signal detection with the optical modulator is ~10%, that is, by comparing the data sets of (a) and (b) shown in Fig. 15. Since the measured rms noise level changed from 1.5 to 0.85 mV, and the optical modulator introduces negligible noise, the signal reduction is due to a

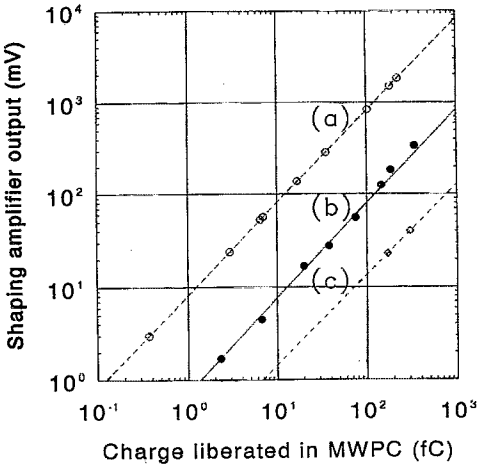

FIG. 15. The linearity of the signal pulse measured with a known amount of charge liberated in the MWPC. The data points of (○), (●), and (◇) are obtained using the three charge measurement schemes shown in Fig. 4(a)–4(c), respectively. Lines are connected for clarity.

lower overall gain of scheme (c). Such signal loss, however, can be recovered by simply adding one more stage of amplifier at the output end. Another better approach would be to increase the signal level by raising the optical drive power from 1 mA of photocurrent to 9 mA. To make the optical modulator more competitive, using devices with a lower V_π and increasing the optical drive power would further enhance its performance.

Finally, in the arrangement shown in Fig. 11(c), cathode charge in the MWPC is injected directly onto the electrode of the optical modulator through a 1 μF high-voltage by-pass capacitor. Although this scheme is impractical for most detector applications because of the generally small signal charges involved, it is nevertheless an alternative approach. An identical photodetector–receiver arrangement to the one described in Sec. II is employed. Figure 13(c) shows a signal pulse of 43 mV when 200 fC of charge is induced on the cathode electrode of the MWPC. The dotted line depicts a typical single signal pulse, while the solid line is an average over 64 signal pulse traces. Unlike the two previous detection arrangements, a large noise level, σ_{rms}=23 mV, is measured. We attribute this large induced noise to the noise voltage pickup by the cathode wire of the MWPC and the excess length of electrical cable (~1 m of BNC cable) connecting the MWPC to the optical modulator. This latter hypothesis is confirmed by removing the attaching cable; significant noise reduction is observed. Comparing the three schemes of charge detection, the collection efficiency of this direct charge injection is 2% to that of the conventional approach; see Fig. 15.

IV. RADIATION HARDNESS

At the completion of the above-mentioned experiments, the optical modulator was exposed to a dose of up to 100 Mrad Co^{60} gamma rays at the rate of 90 krad/h. The ionization induced optical loss was monitored *in situ*. The photon source was a single-mode 1.3 μm LED (Epitaxx) powered by a constant current of 50 mA emitting 9 μW of power output at room temperature. After coupling to a 15 m long polarization maintaining fiber, the emitted light was coupled to the optical modulator by a standard fiber coupler. The light output of the modulator was received by a photodiode after passing through to a 10 m long single-mode fiber. The optical modulator was placed 1 in. away from the opening of a Co^{60} gamma-ray source. A ±10 V triangular wave was applied to the rf port of the optical modulator and with the dc port grounded. The transfer characteristics were then monitored *in situ* every hour. By recording the transfer function, the insertion loss was calculated. It should be noted that by monitoring the signal transfer characteristics, as opposed to measuring the optical transmission at a single dc-bias point, any change in insertion loss as a result of optical phase drift caused by temperature variations can be isolated. A reference single-mode fiber was coirradiated next to the optical modulator to monitor the insertion loss induced by the gamma rays due only to the input and the output fibers. The induced insertion loss measured from the optical modulator was then normalized. This data is plotted in Fig. 16. Within the experimental accuracy (the optical photon source has a long-term

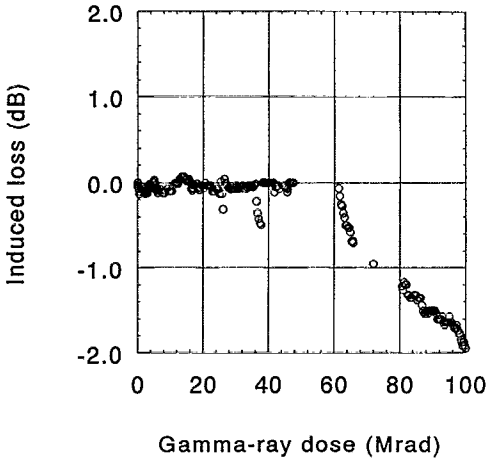

FIG. 16. *In situ* measurement of the gamma-ray ionization induced insertion loss of the optical modulator. The radiation source is Co^{60} emitting at a dose rate of 90 krad/h.

optical power variation of 0.2 dB), the test results show little change in insertion loss, less than 0.2 dB variation, up to a dose of 50 Mrad. However, beyond this radiation level the dielectric components on the optical modulator, including the substrate of the microstrip transmission line and the dielectric materials of the SMA coaxial connector, gradually deteriorated. The combined effects contributed close to 2 dB of insertion loss at a total dose of 100 Mrad.

V. DISCUSSION

One of the main purposes of introducing the optical modulator at the front end of a particle detector is to eliminate the massive amount of electronic devices and cables. However, it is important to understand that the charge gain of an optical modulator is not nearly as high as that of a conventional three-terminal device, such as a transistor. We will carry out this clarification by first briefly reviewing the concept of charge control in an amplifying device. Much insight on the limits of detection sensitivity can be gained by comparing the charge control concept[13] of an optical modulator to that of a transistor.

In a charge-sensitive amplifier device, the increment of the induced charge at the input (δq_{in}) changes the state of the device, and thereby the output current, so that the charge in the output circuit (δq_{out}) increases with accumulation time. To maximize the signal-to-noise ratio for a measurement, the amplifying device is followed by a filter, which in effect determines the averaging time for the noise. The *charge gain* of this device is proportional to the time duration of the measurement t_m;

$$\frac{\delta q_{\text{out}}}{\delta q_{\text{in}}}=\frac{t_m}{\tau}, \tag{5}$$

where τ is the characteristic time constant of the device. In an optimized measurement, the lower limit on the charge sensitivity is the noise of the amplifier $\sigma_{\text{in}}(V)$. These two parameters, charge gain and noise, are important and usually serve as a figure of merit in evaluating the performance of a front end electronic amplifier device. In the case of optical modulator, the time constant τ_A is proportional to the electrode capacitance C_M and the half-wave voltage, and is given by

$$\tau_A=\frac{Q_\pi}{\pi n_0 e}=\frac{Q_\pi}{\pi I_0}=\frac{C_M V_\pi}{\pi I_0}. \tag{6}$$

Using a modulator that has a half-wave voltage of 5 V and electrode capacitance of 5 pF at a photocurrent $I_0=1$ mA, the charging time τ_A is ~8 ns. The corresponding equivalent noise voltage is given in Eq. (4); that is,

$$\sigma_{\text{in}}^A(V)=\frac{V_\pi}{\pi}\sqrt{\frac{a_{F_A}}{n_0 t_{m_A}}}. \tag{7}$$

This expression is to be compared to that of a transistor. In a three-terminal device, such as a bipolar transistor, the time constant is given by

$$\tau_B=\frac{C_B}{g_m}=\frac{C_B kT/e}{I_0}, \tag{8}$$

where C_B is the charge control capacitance of the device, and is defined as a change in the control charge (in the base of the transistor) associated with a change in voltage, g_m the transconductance, e the electron charge, k the Boltzmann constant, and T the temperature. With a typical value of $C_B=5$ pF for a transistor, $kT/e=0.025$ eV at room temperature, and also 1 mA of carrying current (collector current), the time constant τ_B is 0.125 ns, while the equivalent noise voltage of a three-terminal device is given by

$$\sigma_{\text{in}}^B=\frac{kT}{e}\sqrt{\frac{a_{F_B} e}{I_0 t_{m_B}}}=\frac{kT}{e}\sqrt{\frac{a_{F_B}}{n_0 t_{m_B}}}. \tag{9}$$

Comparing the time constants of the two schemes, the charge gain of a bipolar transistor is 64× higher, that is, $\tau_A/\tau_B=8$ ns/0.125 ns, than that of an optical modulator when the measurement times t_{m_A} and t_{m_B} are set equal. The noise of a transistor is also lower than that of an optical modulator by a factor of 63.7, that is $\sigma_{\text{in}}^A/\sigma_{\text{in}}^B=(V_\pi/\pi)/(kT/e)$. Therefore the half-wave voltage of the optical modulator would have to be lowered substantially in order for the modulator to approach the sensitivity of electronic devices. We conclude that to utilize the advantages of small size, low mass–volume, large bandwidth handling capability, and high radiation tolerance of Ti:$LiNbO_3$ optical modulators, a preamplifier is needed between the particle detector and the optical modulators if signal-to-noise ratio is important.

Although optical modulators have shown a great promise for the readout of particle detector signals,[1–3,14] like many other newly developed technologies, there are some obstacles to be overcome before such optical readout schemes can become a reality. Some of the engineering aspects includes reducing the dc thermal drift of the optical modulator, improving the sensitivity by lowering the V_π value, eliminating the need for a polarization maintaining fiber at the input end, development of an universal optical-fiber-array cold feedthrough with low insertion loss, optimizing the optical power by minimizing the number of optical fan-outs per signal channel and reducing the numbers of optical power dis-

tribution notes, and, finally, lowering the cost by monolithically integrating optical modulators with supporting electronics. It is interesting to note that these engineering aspects are in fact general if any form of optical schemes are to be used on large scale in particle detectors. In recent years, some of this technical aspects have been addressed and the results are encouraging. It is clear that the sophistication of optical techniques to come and the quest for larger and faster data transfer would change the traditional signal transfer techniques based on electronics in particle detectors to opto-electronics.

Recently, much effort to fabricate intensity optical modulators using various semiconductor materials other than the conventional Ti:$LiNbO_3$ waveguide structure is reported.[15–18] It is hoped that using the state-of-the-art fabrication technology, optical modulators and other electronics may be integrated together to improve the performance and lower the cost. But unlike optical systems used in telecommunications where digital signals are predominantly transferred, particle detector signals are predominantly analog where a large dynamic range and good linearity are required. Furthermore, the imperative requirement of radiation hardness compounds the problem. Although optical modulators using MQW structures seem to be fairly radiation hard, much improvement is needed on the linearity and dynamic range. Silcon and polymer MZ-type optical modulators are still very much at the early stage of development.[19] However, one should not overlook the potential of intensity optical modulators based on semiconductors for detector signal transfer.

ACKNOWLEDGMENTS

We thank Bo Yu and Graham Smith for assisting us on the charge measurements using the MWPC and William Willis and Michael Seman of the Columbia University for their efforts and equipment on loan, and appreciate the technical assistance of Jim Kierstead, Joe Mead, Jr., Lee Rogers, John Schill, and Dmitri Stephani. This research is supported by the US Department of Energy under Contract No. DE-AC35-89ER40486 and No. DE-AC02-76CH00016.

[1] T. Tsang, V. Radeka, T. Srinivasan-Rao, and W. Willis, *Symposium on Detector R&D for the Superconducting Super Collider, Fort Worth, Texas, 1990*, edited by T. Dombeck, V. Kelly, and G. P. Yost (World Scientific, Singapore, 1990), p. 491.
[2] E. Ables, R. Bionta, M. Lowry, D. Masquelier, K. McCammon, C. McConaghy, and C. Wuest, Nucl. Instrum. Methods A **316**, 452 (1992).
[3] G. Stefanini, C. DaVia, J. Feyt, P. Nappey, J. Dowell, P. M. Hattersley, R. J. Homer, P. Jovanovic, I. Kenyon, R. Staley, K. Webster, B. Dwir, M. Glick, F. K. Reinhart, J. Davies, N. Green, W. Stewart, T. Young, G. Hall, T. Akesson, G. Jarlskog, S. Kröll, R. Nickerson, and S. Jaroslawski, CERN DRDC 93–95/RD 23 Status Report, 1993.
[4] K. K. Wong, Proc. SPIE **993**, 13 (1988); J. L. Jackel, C. E. Rice, and J. J. Veselka, Appl. Phys. Lett. **51**, 607 (1982); A. Loni, Laser Focus World **27**, 183 (1991).
[5] M. L. Farwell, *et al.*, IEEE Photon. Tech. Lett. **3**, 792 (1991).
[6] G. S. Maurer, P. W. Cornish, and R. A. Becker, Proceedings of the Optical Fiber Committee, paper No. ThI5, 1991.
[7] S. Yamada and M. Minakata, Jpn. J. Appl. Phys. **20**, 733 (1981).
[8] P. Skeath, C. H. Bulmer, S. C. Hiser, and W. K. Burns, Appl. Phys. Lett. **49**, 1221 (1986).
[9] H. Nagata and K. Kluchi, J. Appl. Phys. **73**, 4162 (1993).
[10] H. Nagata, K. Kluchi, S. Shimotsu, J. Ogiwara, and J. Minowa, J. Appl. Phys. **76**, 1405 (1994).
[11] E. D. Jungbluth, Laser Focus World **29**, 85 (1993).
[12] C. H. Bulmer and W. K. Burns, Appl. Phys. Lett. **48**, 1036 (1986).
[13] V. Radeka, Ann. Rev. Nucl. Sci. **38**, 217 (1988).
[14] R. A. Becker and B. E. Kincaid, Appl. Opt. **32**, 6690 (1993).
[15] H. Robinson, C. W. Pitt, and R. A. Gibson, Appl. Opt. **32**, 3981 (1993).
[16] M. A. Haase, H. Cheng, D. K. Misemer, T. A. Strand, and J. M. DePuydt, Appl. Phys. Lett. **59**, 3228 (1991).
[17] E. Bigan, M. Allovon, M. Carre, and P. Voisin, Appl. Phys. Lett. **57**, 327 (1990).
[18] S. Cheung, F. Jain, R. Sacks, D. Cullen, G. Ball, and T. Grudkowski, Appl. Phys. Lett. **63**, 296 (1993).
[19] R. A. Mayer, K. H. Jung, W. D. Lee, D. Kwong, and J. C. Campbell, Opt. Lett. **17**, 1812 (1992); K. W. Goossen, J. E. Cunningham, A. E. White, K. T. Short, W. Y. Jan, and J. A. Walker, IEEE Photon. Tech. Lett. **4**, 140 (1992); T. A. Tumolillo, Jr. and P. R. Ashley, Appl. Phys. Lett. **62**, 3068 (1993); F. Ebisawa, M. Hoshino, and K. Sukegawa, *ibid.* **65**, 2919 (1994); D E. Bossi and R. W. Ade, Laser Focus World **28**, 135 (1992).